Model-Based Knowledge-Driven Learning Approach for Enhanced High-Resolution Automotive Radar Imaging

Ruxin Zheng, *Student Member, IEEE*, Shunqiao Sun, *Senior Member, IEEE*, Hongshan Liu, *Student Member, IEEE*, Honglei Chen, *Member, IEEE*, and Jian Li, *Fellow, IEEE*

***Abstract*—Millimeter-wave (mmWave) radars are indispensable for perception tasks of autonomous vehicles, thanks to their resilience in challenging weather and light conditions. Yet, their deployment is often limited by insufficient spatial resolution for precise semantic scene interpretation. Classical super-resolution techniques adapted from optical imaging inadequately address the distinct characteristics of radar data. In response, our study herein redefines super-resolution radar imaging as a one-dimensional (1D) signal super-resolution spectra estimation problem by harnessing the radar domain knowledge, introducing innovative data normalization, signal-level augmentation, and a domain-informed signal-to-noise ratio (SNR)-guided loss function. Like an image drawn with points and lines, radar imaging can be viewed as generated from points (antenna elements) and lines (frequency spectra). Our tailored deep learning network for automotive radar imaging exhibits remarkable scalability and parameter efficiency, alongside enhanced performance in terms of radar imaging quality and resolution. We further present a novel real-world dataset, pivotal for both advancing radar imaging and refining super-resolution spectra estimation techniques. Extensive testing confirms that our SR-SPECNet sets a new benchmark in producing high-resolution radar range-azimuth images, outperforming existing methods. The source code and radar dataset utilized for evaluation will be made publicly available at https://github.com/ruxinzh/SR-SPECNet.**

***Index Terms*—Automotive Radar, High-Resolution Radar Imaging, Real-World Dataset, Direction-of-Arrival Estimation, Deep Learning**

I. Introduction

Radar technology, particularly in the form of millimeter wave radars, has become a cornerstone for advanced driver assistance systems (ADAS) and autonomous vehicles, surpassing the capabilities of traditional RGB cameras and LiDAR in challenging weather and low visibility conditions [1]–[9]. Its adoption is largely driven by the robust, cost-effective, and reliable sensing solutions it offers, operational under virtually all environmental scenarios. Frequency-modulated continuous-wave (FMCW) signals within the millimeter-wave band are primarily utilized in these radar systems, chosen for their cost-efficient operation and potential for high-resolution sensing. Much like an exquisite image woven from points and lines, radar imaging emerges from the harmonious interplay of antenna elements as points and frequency spectra as lines. Radar sensing is pivotal for a broad spectrum of autonomous driving functionalities, including free space detection, 360° surrounding sensing, object detection and classification, and simultaneous localization and mapping (SLAM) [10]–[12].

Historically, the automotive radar technology, dating back to the late 1990s and early 2000s, was developed with a focus on supporting ADAS functions like adaptive cruise control (ACC) [4]. However, these radar systems primarily measure speed and range, offering limited azimuth angular resolution. Level 4 and 5 fully autonomous driving demands four-dimensional (4D) high-resolution sensing [10]. Such advanced sensing is essential for speed, range determination and for accurately estimating targets' azimuth and elevation angles with high resolution. Figure 1 illustrates how antenna aperture and super-resolution algorithms influence the quality of range-azimuth (RA) heatmaps. The high-resolution RA heatmaps contain rich information of the objects, including their shapes, facilitating object detection and classification through using deep neural networks [7].

The challenge of enhancing angular resolution has led to the standardization of the multiple-input multiple-output (MIMO) radar technology. MIMO radar forms a large virtual aperture through exploiting waveform diversity, significantly improving angular resolution with a manageable number of transmit and receive antennas [3], [13]–[15]. Further, signal processing techniques have been explored to further improve the angular resolution beyond what is achievable through digital beamforming implemented via fast Fourier transform (FFT). Super-resolution direction-of-arrival (DOA) estimation algorithms, such as compressive sensing (CS) [16]–[18] and the iterative adaptive approach (IAA) [19], [20], have made notable advancements in this area. Yet, their computational demand presents a formidable barrier to real-time implementation in automotive radars with embedded digital signal processors.

The adoption of deep learning (DL) techniques for radar image enhancement has yielded significant advances within the realm of image super-resolution, as demonstrated in computer vision research [21]–[23]. Applying these methods to enhance azimuth resolution in RA heatmaps presents significant potential for substantial improvement. Nonetheless, few studies have focused on generating super-resolution RA heatmaps using raw radar signals by exploiting radar domain knowledge. Approaches that consider generating radar super-resolution

The work of R. Zheng, S. Sun and H. Liu was supported in part by U.S. National Science Foundation (NSF) under Grants CCF-2153386, ECCS-2033433, and Alabama Transportation Institute (ATI).

R. Zheng, S. Sun and H. Liu are with the Department of Electrical and Computer Engineering, The University of Alabama, Tuscaloosa, AL, USA (emails: rzheng9@crimson.ua.edu, shunqiao.sun@ua.edu).

H. Chen is with Mathworks, Inc, Natick, MA, USA (email: hchen@mathworks.com)

J. Li is with the Department of Electrical and Computer Engineering, University of Florida, Gainesville, FL, USA (email: li@dsp.ufl.edu)

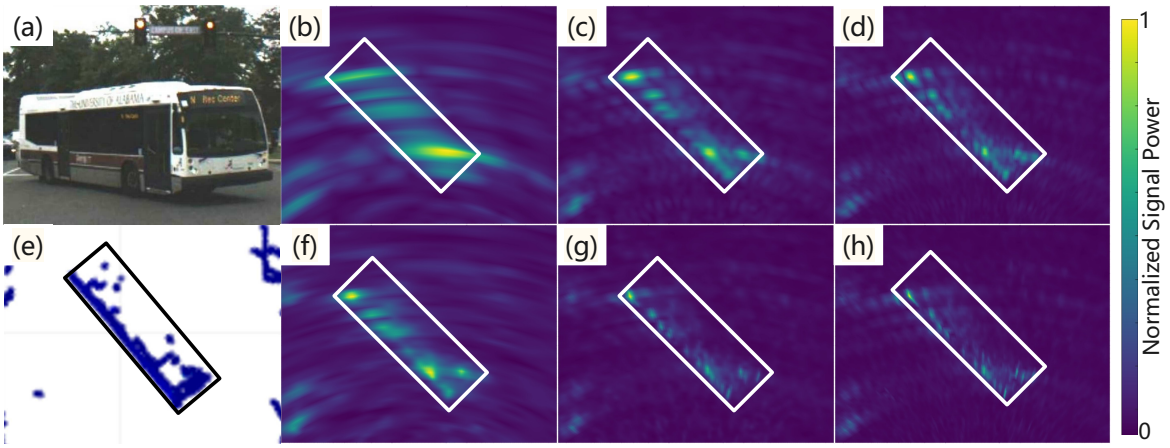

Figure 1: Impact of antenna aperture and super-resolution algorithms on RA heatmap quality: (a) shows an RGB bus image. RA heatmaps using FFT for (b) 10, (c) 40, and (d) 86 antennas contrast with (e) LiDAR bird eye view (BEV). Heatmaps with IAA for (f) 10, (g) 40, and (h) 86 antennas highlight the improved clarity from both antenna count and super-resolution algorithm.

RA heatmaps as straightforward image-to-image or volume-to-volume tasks often overlook the critical domain knowledge of radar signal processing [22], [23]. This oversight can lead to data-intensive solutions, reliance on excessively large networks that lack explainability, an aspect particularly important in safety-critical applications—or fail to deliver optimal performance and scalability, both of which are key concerns in autonomous driving applications where rapid inference and compact model size are essential for on-chip implementations.

Research in the domain of super-resolution RA heatmap generation for automotive radar remains limited, with the majority of studies relying on FFT-generated ground truths from larger antenna arrays [22], [23]. To the best of our knowledge, no existing methods leverage RA heatmaps produced through using super-resolution algorithms as ground truths. This paper addresses these gaps by introducing the Super-Resolution Angular Spectra Estimation Network (SR-SPECNet). Built upon a deep integration of radar signal processing domain knowledge, SR-SPECNet significantly advances the generation of super-resolution angular spectra. By transforming RA heatmap enhancement into a more tractable 1D azimuth super-resolution problem, SR-SPECNet efficiently harnesses radar-specific insights to enhance performance while maintaining model interpretability, which is crucial for safety-critical applications. This transformation is supported by our novel data normalization approach, signal-level augmentation and a signal-to-noise ratio (SNR)-guided loss function. We evaluate SR-SPECNet extensively using both our proprietary real-world dataset and publicly available dataset. Our experimental analysis demonstrates that SR-SPECNet offers exceptional parameter efficiency, superior imaging quality, and remarkable scalability, consistently outperforming established benchmarks.

The key contributions of our work include:

- We present SR-SPECNet, a radar-domain knowledge-driven network engineered for both efficiency and effectiveness. SR-SPECNet leverages single-snapshot measurements to deliver high-resolution automotive RA imaging, comparable to that typically achieved through IAA with a large radar array aperture. However, it surpasses IAA by offering superior performance while significantly reducing computational costs.
- We introduced novel signal augmentation methods and leveraged domain knowledge from radar signal processing to guide neural network design, demonstrating SR-SPECNet's scalability, efficiency, and robust performance. This approach involves conceptualizing RA imaging as a 1D spectral estimation problem, introducing an innovative normalization method for real radar data, and implementing a SNR-guided loss function.

The remainder of this paper is organized as follows. We first review related work, including super-resolution DOA estimation algorithms (both model-based and DL-based), current methods for improving radar RA heatmap resolution, and existing automotive radar datasets, along with an introduction to our own dataset. We then present SR-SPECNet, beginning with the system model for DOA estimation and the IAA algorithm, followed by the SR-SPECNet architecture inspired by IAA. This section also covers data preprocessing, signal-level augmentation, and the SNR-guided loss function. Finally, the experimental section details the benchmark networks, evaluation metrics, implementation specifics, and performance evaluation, with visualizations of SR-SPECNet's outputs to highlight its effectiveness.

II. Related Work

Efforts to enhance radar imaging have primarily focused on improving azimuth resolution, especially due to limited antenna elements, as range resolution is typically improved by increased bandwidth. This section reviews super-resolution algorithms for spectral estimation, including both model-based and deep learning (DL)-based methods, deep learning enable super-resolution approaches, and radar datasets.

A. Super-Resolution Algorithms

1) Model-Based Approaches: The evolution of DOA estimation methodologies has been marked by significant milestones over the past decades, with substantial advancements in both theory and application [24], [25]. In the automotive radar domain, digital beamforming (DBF) has emerged as the predominant DOA estimation algorithm, favored for its computational efficiency and robustness. This technique, typically implemented via FFT, however, faces limitations in angular resolution due to the Rayleigh criterion and is characterized by relatively high sidelobes [3], [26].

Automotive radars, operating within highly dynamic environments, often have access to only a limited number of snapshots, sometimes as few as a single snapshot. This scenario renders traditional super-resolution methods, such as Capon beamforming, MUSIC [27], and ESPRIT [28], which require multiple snapshots for accurate covariance matrix estimation, less viable.

Compressive sensing (CS) techniques [16], [18], which exploit the sparsity of target distributions in the angular domain, have shown exceptional super-resolution capabilities and are notably effective in snapshot-constrained settings. However, CS methods require the dictionary matrix to have low mutual coherence.

On the contrary, the iterative adaptive approach (IAA) [19], [20] offers a robust DOA estimation performance under limited snapshots, utilizing an iterative, nonparametric methodology. However, IAA has high computational complexity, involving large dimensional matrix inversions in each iteration. Efforts to mitigate these computational challenges have led to the development of fast algorithms, including fast IAA [29], [30], and super fast IAA [31]. Yet, the computational overhead remains considerable.

2) DL-Based Approaches: Unlike the model-based approaches, which are based on simple mathematical models that are hand-designed from domain knowledge, DL-based approaches currently prevalent to replace simple principled models with purely data-driven pipelines, trained with massive labeled datasets. The DL-based DOA estimation approaches have been shown to have rapid inference, enhanced super-resolution capabilities, and robustness in low SNR conditions [32]–[37].

In terms of network output, the DL-based approaches can be broadly classified into two categories. The first category addresses DOA estimation as a binary classification challenge, determining the presence or absence of targets across a discretized angle grid. However, as the grid resolution increases and the number of potential targets grows, the combinations of possible target angles increase exponentially. This results in challenges such as unbalanced training data and significant hardware demands, making the training dataset excessively large and the network impractical to train. In contrast, the second category approaches DOA estimation through a regression framework, producing continuous line spectra. The latter method proves particularly beneficial for generating continuous spectra, which are crucial for creating detailed RA heatmaps.

Moreover, the process of collecting and labeling automotive radar data necessary for training these systems is both costly and labor-intensive, posing additional challenges to the development and deployment of robust DOA estimation models.

3) Model-Based DL Approaches: Purely data-driven approaches to DOA estimation often suffer from limited interpretability and require extensive datasets for effective training. To address the challenges associated with traditional model-based methods and the lack of transparency in black-box deep learning systems, model-based deep learning techniques have been developed. These techniques integrate the strengths of signal processing and machine learning, benefiting from both domains [25], [49], [50].

Prominent examples of model-based deep learning approaches include algorithm unrolling [51] and plug-and-play networks [49], [52]. These hybrid methods merge mathematical optimization models with the flexibility of data-driven frameworks, leveraging domain-specific knowledge and mathematical structures to offer a principled and interpretable solution [49], [53]–[58].

Despite these advances, current DL-based and model-based deep learning approaches rely heavily on oversimplified simulated datasets, typically consisting of point targets such as light poles. These datasets fail to capture the complexity of real-world automotive radar scenarios, which often involve extended targets like trucks and multiple scatterers such as buildings. Furthermore, many existing methods require multiple snapshots as input, while automotive radar systems often have access to only limited or even single-snapshot data. To the best of our knowledge, no existing network has been trained or tested on real-world single-snapshot automotive radar data for DOA estimation purposes.

B. Enhance Radar-Based Imaging Resolution

Recently, deep learning techniques have been employed to tackle the challenges of enhancing resolution in radar-based imaging. An adversarial network was tailored for super-resolution in micro-Doppler imagery [21], showcasing the potential of generative adversarial networks (GANs) in radar image enhancement. A U-Net architecture was employed for the super-resolution of weather radar maps [22], demonstrating the adaptability of deep convolutional networks to various radar data modalities. Notably, [23] ventured into extrapolating received antenna signals through a compact network, followed by the application of a 3D U-Net on the range-Doppler-azimuth data cube, facilitating the generation of super-resolution RA heatmaps. However, the existing body of work primarily leverages 2D or 3D network architectures, predicated on the assumption that the problem space necessitates multi-dimensional data processing to achieve enhanced resolution. This perspective, while valid, overlooks the potential efficiencies and novel insights that can be garnered from reinterpreting the challenge through a one-dimensional lens. To our best knowledge, no prior work has endeavored to address radar azimuth super-resolution within RA heatmaps using a 1D approach.

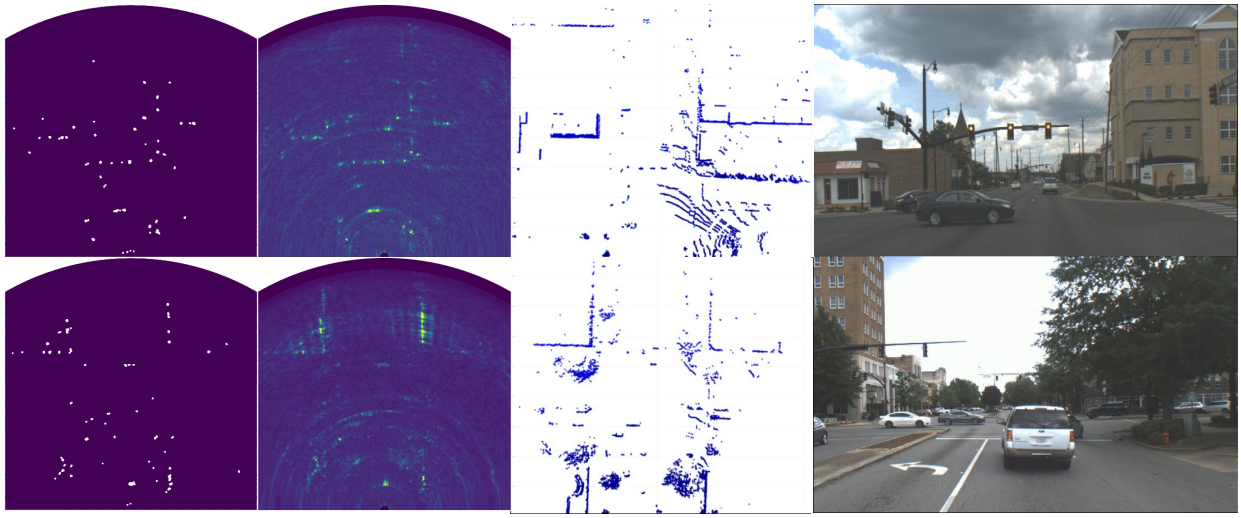

Figure 2: Left to right columns: radar point clouds, RA maps in Cartesian coordinates, LiDAR point clouds in bird's-eye view, and camera image.

Dataset	# of Frames	Data Type	Resolution	Radar/Technology
nuScenes [38]	40,000	Sparse PC	Low	Continental ARS408
Oxford Radar [39]	240,000	RA	High	Navtech Spinning Radar
RADIATE [40]	44,000	RA	High	Navtech Spinning Radar
CRUW [41]	396,241	RA	Low	TI AWR1843
Zendar [42]	94,460	ADC,RD,PC	High	SAR
CARRADA [43]	12,666	RA,RD,RAD	Low	TI AWR1843
RadarScenes [44]	975	Dense PC	High	77GHz Middle-Range Radar
RADIal [45]	25,000	ADC,RD,PC	High	Valeo Middle Range DDM
View-of-Delft [46]	8,693	PC+Doppler	High	ZF FRGen21 Radar
K-Radar [47]	35,000	4D Tensor	High	KAIST-Radar
Radatron [48]	152,000	4D Tensor	High	TI Cascade Imaging Radar
Ours	17,000	ADC	High	TI Cascade Imaging Radar

Table I: Overview of publicly available radar data sets. Data Type: Raw ADC data (ADC), Range-Doppler map (RD), Range-Azimuth map (RA), point clouds (PC).

C. Radar Datasets

Automotive radar machine learning heavily relies on high-quality radar data to ensure accurate model training and robust performance in real-world applications. As shown in Table I, CARRADA and CRUW datasets employ single-chip Texas Instruments (TI) radar systems, offering modest angular resolutions exceeding 10°. Technologies like spinning radar, utilized in the RADIATE and Oxford Radar RobotCar datasets, provide high-resolution 360-degree field-of-view (FOV) imagery, albeit at limited frame rates, which can introduce motion blur challenges. The Zendar dataset, leveraging synthetic aperture radar (SAR) technology, excels in imaging static targets by integrating measurements from different vehicle positions. The View-of-Delft dataset takes advantage of the ZF FRGen21 radar's long-range and high-resolution imaging capabilities [59], offering point cloud data with object annotations confined to a 50 meter range.

In this paper, we curate our own radar dataset for the proposed model-based, knowledge-driven network, which necessitates detailed radar configuration parameters and extensive raw analog-to-digital converter (ADC) data processing to seamlessly integrate super-resolution algorithms and assess network performance across various antenna apertures. The centerpiece of our dataset is the TI cascaded imaging radar system [60], mounted on a Lexus RX450h SUV, together with other sensing modalities, including Teledyne FLIR Blackfly S stereo cameras, and a Velodyne Ultra Puck VLP-32C LiDAR sensor. The radar is configured for MIMO operations with an array of 12 transmit and 16 receive antennas, synthesizing a virtual uniform linear array (ULA) of 86 elements, with half-wavelength spacing, rendering an azimuth resolution of roughly 1.2° via FFT. As illustrated in Fig. 2, our dataset showcases the exceptional high-resolution capabilities.

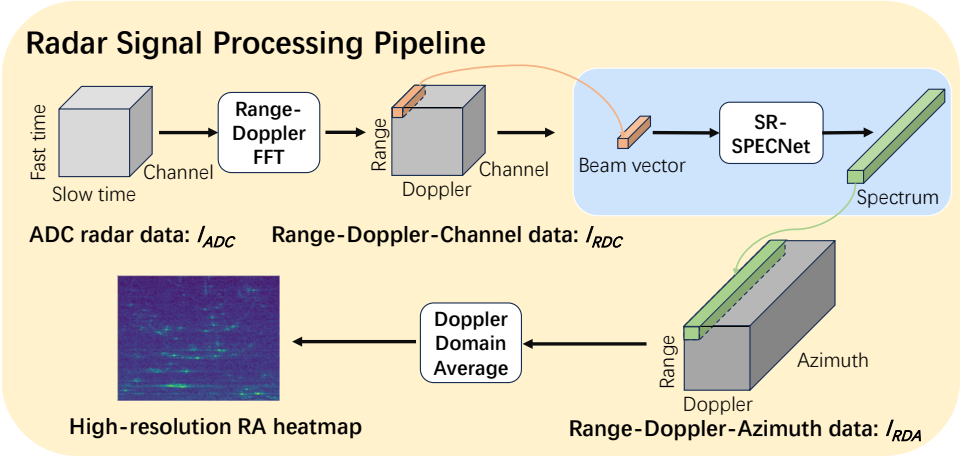

Figure 3: The signal processing pipeline of high-resolution radar imaging.

III. Super-Resolution Angular Spectra Estimation Network (SR-SPECNet)

In this section, we present a model-based, knowledge-driven neural network approach to transform raw ADC data into high-resolution RA maps. In contrast to recent methods that derive high-resolution ground truth from RA maps using an expanded antenna array [23], our approach additionally utilizes RA maps refined through IAA algorithms, serving as our ground truth.

A. System Model

The proposed high-resolution radar imaging signal processing flow with SR-SPECNet is shown in Figure 3. The input ADC data, $I_{\text{ADC}} \in \mathbb{C}^{N_{\text{fast}} \times N_{\text{slow}} \times N_{\text{ch}}}$, encapsulates three dimensions: N_{fast} for fast time samples, N_{slow} for slow time samples (or chirps), and N_{ch} for channels (or receivers). Through a 2D FFT to I_{ADC} across both fast and slow time dimensions, we obtain range-Doppler-channel data, $I_{\text{RDC}} \in \mathbb{C}^{N_{\text{Range}} \times N_{\text{Doppler}} \times N_{\text{ch}}}$. Subsequently, beam vectors $\mathbf{y} \in \mathbb{C}^{1 \times 1 \times N_{\text{ch}}}$ are extracted from each range-Doppler bin. These vectors are processed by SR-SPECNet to generate a super-resolution spectrum. This operation, performed on all beam vectors across all range-Doppler bins, yields the range-Doppler-azimuth data, $I_{\text{RDA}} \in \mathbb{R}^{N_{\text{Range}} \times N_{\text{Doppler}} \times N_{\text{Azimuth}}}$. Notably, this procedure is highly parallelizable, treating the dataset as a 2D matrix with a batch size of $N_{\text{Range}} \times N_{\text{Doppler}}$. The final high-resolution RA maps, $M \in \mathbb{R}^{N_{\text{Range}} \times N_{\text{Azimuth}}}$, are achieved by averaging I_{RDA} over Doppler dimension.

To facilitate the introduction of our proposed model-based, knowledge-driven neural network approach, we first present the array model and super-resolution spectral estimation. Let's consider a scenario with K narrowband far-field source signals s_k for $k = 1, \cdots, K$, are incident upon a linear, omnidirectional antenna array consisting of N elements. These signals arrive from directions θ_k for $k = 1, \cdots, K$. The temporal differences among the sensors can be accurately captured through simple phase shifts, resulting in the following data model

$$\begin{aligned} \mathbf{y}(\mathbf{t}) &= \sum_{k=1}^{K} \mathbf{a}(\theta_k) s_k(k) + \mathbf{n}(t) \\ &= \mathbf{A}(\boldsymbol{\theta})\mathbf{s}(t) + \mathbf{n}(t), \quad t = 1, \cdots, T, \end{aligned} \tag{1}$$

where t denotes the snapshot index, $\mathbf{n}$ is a complex $N \times 1$ white Gaussian noise vector, and $\mathbf{A}(\boldsymbol{\theta}) = [\mathbf{a}(\theta_1), \mathbf{a}(\theta_2), \cdots, \mathbf{a}(\theta_K)]$ represents the $N \times K$ array manifold matrix. The array response vector $\mathbf{a}(\theta)$ is defined as

$$\mathbf{a}(\theta) = \left[1, e^{\frac{2\pi d_2}{\lambda} \sin\theta}, \cdots, e^{\frac{2\pi d_N}{\lambda} \sin\theta}\right]^T. \tag{2}$$

Here, θ represents the direction of arrival of the signal, d_n indicates the spacing between the n-th element and the first element, while $\mathbf{s} = [s_1, s_2, \cdots, s_K]^T$ denotes the vector of source signals. In this study, our analysis is concentrated on the single snapshot scenario, driven by the highly dynamic environments encountered in automotive radar applications. Therefore, we base our model on a singular snapshot $\mathbf{y}$ of the array's response. With T set to 1, the signal snapshot model simplifies to $\mathbf{y} = \mathbf{A}(\boldsymbol{\theta})\mathbf{s} + \mathbf{n}$.

IAA is a data-dependent, nonparametric algorithm [19]. It discretizes the DOA space into an L point grid, defining the array manifold as $\mathbf{A}(\boldsymbol{\theta}) = [\mathbf{a}(\theta_1), \cdots, \mathbf{a}(\theta_L)]$. The fictitious covariance matrix of $\mathbf{y}$ is represented as $\mathbf{R}_f = \mathbf{A}(\boldsymbol{\theta})\mathbf{P}\mathbf{A}^H(\boldsymbol{\theta})$, where P is a $L \times L$ diagonal matrix with the l-th diagonal element being $p_l = |\hat{s}_l|^2$, and $\hat{s}_l$ is the source reflection coefficient corresponding to direction θ_l.

IAA iteratively estimates the reflection coefficient $\hat{s}$ and updates the fictitious covariance matrix by minimizing the weighted least-square (WLS) cost function $\|\mathbf{y} - s_l\mathbf{a}(\theta_l)\|^2_{\mathbf{Q}^{-1}(\theta_l)}$, where $\|\mathbf{X}\|^2_{\mathbf{Q}^{-1}(\theta_l)} \triangleq \mathbf{X}^H\mathbf{Q}^{-1}(\theta_l)\mathbf{X}$ and $\mathbf{Q}(\theta_l) = \mathbf{R}_f - P_l\mathbf{a}(\theta_l)\mathbf{a}^H(\theta_l)$. The solution to this optimization problem is

$$\hat{s}_l = \frac{\mathbf{a}^H(\theta_l)\mathbf{R}_f^{-1}}{\mathbf{a}^H(\theta_l)\mathbf{R}_f^{-1}\mathbf{a}(\theta_l)}\mathbf{y}. \tag{3}$$

From Equation (3), each iteration of the IAA essentially involves performing MPDR type of beamforming. In IAA, new

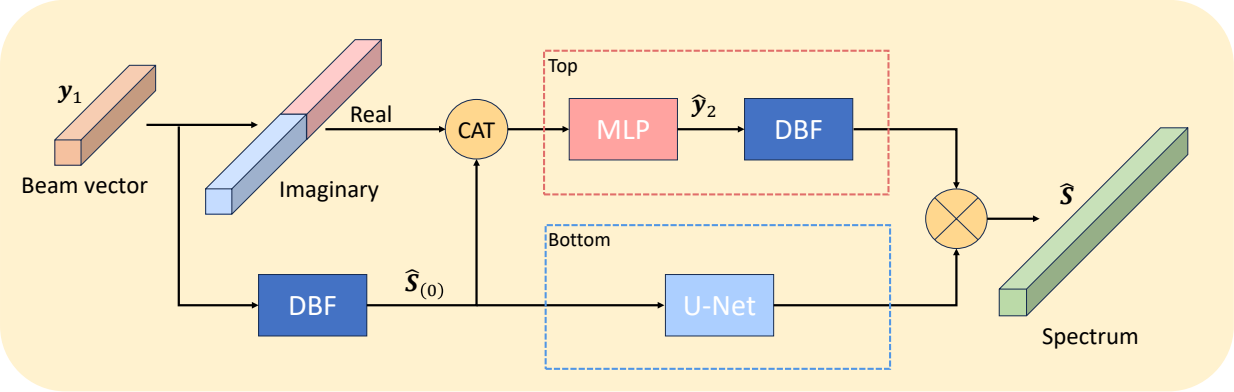

Figure 4: Architecture of SR-SPECNet.

beamformer weights are iteratively calculated, coupled with the application of diagonal loading techniques [61], [62] to the fictitious covariance matrix before matrix inversion, which enhances the algorithm's robustness and stability.

B. SR-SPECNet Architecture

The model-based, knowledge-driven SR-SPECNet is designed with insights from the IAA algorithm. Under IAA, the estimated reflection coefficient at direction θ_l in the n-th iteration can be obtained as

$$\hat{s}_{l(n)} = \frac{\mathbf{a}^H(\theta_l)\mathbf{R}^{-1}_{(n-1)}\mathbf{y}}{\mathbf{a}^H(\theta_l)\mathbf{R}^{-1}_{(n-1)}\mathbf{a}(\theta_l)}. \tag{4}$$

The initial spectrum estimation, which is used to calculate the fictitious covariance matrix $\mathbf{R}(0)$, is initialized using DFT, i.e.,

$$\hat{s}_{l(0)} = \left|\frac{\mathbf{a}^H(\theta_l)\mathbf{y}}{N_{ch}}\right|, \tag{5}$$

where $|\cdot|$ denotes the absolute value. Equation (4) can be further rewritten as:

$$\hat{\mathbf{s}}_{(n)} = T(\hat{\mathbf{s}}_{(n-1)}, \mathbf{y}) \oslash B(\hat{\mathbf{s}}_{(n-1)}), \tag{6}$$

where

$$T(\hat{\mathbf{s}}_{(n-1)}, \mathbf{y}) = \mathbf{A}^H(\boldsymbol{\theta})\mathbf{R}^{-1}_{(n-1)}\mathbf{y}, \tag{7}$$

$$B(\hat{\mathbf{s}}_{(n-1)}) = \mathrm{Diag}\left(\mathbf{A}^H(\boldsymbol{\theta})\mathbf{R}^{-1}_{(n-1)}\mathbf{A}(\boldsymbol{\theta})\right), \tag{8}$$

$$\mathbf{R}_{(n-1)} = \mathbf{A}(\boldsymbol{\theta})\mathrm{diag}\left(\hat{\mathbf{s}}^2_{(n-1)}\right)\mathbf{A}^H(\boldsymbol{\theta}), \tag{9}$$

and $\hat{\mathbf{s}} = \{\hat{s}_1, \hat{s}_2, \cdots, \hat{s}_l\}$. The notation $\mathrm{diag}(\cdot)$ denotes the operation of creating a diagonal matrix from a vector, and $\mathrm{Diag}(\cdot)$ signifies extracting the diagonal elements of a matrix. The symbol $\oslash$ represents element-wise division.

The architecture of SR-SPECNet is illustrated in Fig. 4. The network is designed to enhance spectral resolution in RA imaging by incorporating radar signal processing principles within a deep learning framework. The input to the network is a beam vector $\mathbf{y}_1 \in \mathbb{C}^{N_{\mathrm{ch1}}}$, which represents the received radar signal after range-Doppler processing. Before entering the network, an initial spectrum estimate $\hat{\mathbf{s}}_{(0)}$ is computed using a DFT-based beamforming method. Since SR-SPECNet processes only real-valued inputs, the real and imaginary components of $\mathbf{y}_1$ are separated and concatenated with $\hat{\mathbf{s}}_{(0)}$, ensuring that the network preserves essential spectral and phase information necessary for accurate DOA estimation.

SR-SPECNet is structured to explicitly mirror IAA, decomposing the spectral estimation process into two primary components: a top network that learns the transformation $T(\hat{\mathbf{s}}_{(0)}, \mathbf{y}_1)$, and a bottom network that approximates the normalization function $B(\hat{\mathbf{s}}_{(n-1)})$. This structured decomposition allows the network to incorporate domain knowledge from IAA, ensuring that it operates as a model-driven hybrid rather than a purely data-driven deep learning model.

1) Top Network: The transformation $T(\hat{\mathbf{s}}_{(0)}, \mathbf{y}_1)$ involves the inversion of the covariance matrix, which is then used to compute a beamforming weight matrix. This transformation is inherently global in nature, as each output element depends on all elements of the input. The top network employs a multilayer perceptron (MLP) to approximate this transformation while simultaneously mapping the input beam vector from N_{ch1}, a lower-dimensional space, to N_{ch2}, a higher-dimensional space, which corresponds to the resolution of the IAA-based ground truth spectra. The dimensionality expansion performed by the MLP is a critical aspect of SR-SPECNet, as it ensures that the output beam vector $\hat{\mathbf{y}}_2 \in \mathbb{C}^{N_{\mathrm{ch2}}}$ matches the resolution required for high-fidelity spectral reconstruction. This mapping not only approximates the inverse covariance transformation but also performs a structured extrapolation that effectively expands the array aperture from the input beam vector, enhancing spatial resolution.

Additionally, the transformation performed by the top network involves nonlinear mappings that are not adequately captured by traditional beamforming techniques. The nonlinearity introduced by the activation functions in the MLP enables the network to approximate complex mappings required for spectral enhancement. Unlike CNNs, which assume that adjacent input elements are related through local spatial structures, an MLP does not rely on locality assumptions and can effectively model global dependencies across the entire beam vector. After processing by the MLP, DBF is applied to $\hat{\mathbf{y}}_2$, forming the final output of the top network. This transformed representation corresponds to the numerator in the IAA formulation, ensuring

that spectral enhancement is applied in accordance with the learned inverse covariance transformation.

2) Bottom Network: The bottom network is designed to approximate the function $B(\hat{\mathbf{s}}_{(n-1)})$, which acts as a normalization term in IAA, adjusting the spectral estimates to ensure stability and robustness against noise. This function scales the spectral estimates in a locally structured manner, ensuring that peaks corresponding to true targets are properly emphasized relative to surrounding noise and sidelobes. Since this function inherently captures local spectral relationships, the bottom network adopts a 1D U-Net [63] architecture, which is well suited for refining spectral estimates while preserving fine-scale structures.

The 1D U-Net is particularly advantageous due to its ability to extract spectral patterns at multiple scales while maintaining spectral coherence. Its encoder-decoder structure facilitates multi-scale feature refinement, ensuring that spectral estimates remain stable and physically interpretable. Moreover, the U-Net preserves the input-output dimensionality, aligning naturally with the properties of $B(\hat{\mathbf{s}}_{(n-1)})$ in IAA. The skip connections within the U-Net play a crucial role in retaining fine spectral details and preventing information loss during encoding and decoding, which is particularly beneficial for mitigating sidelobes and enhancing the clarity of the reconstructed RA heatmaps. By leveraging convolutional feature extraction, the U-Net effectively models the structured nature of the IAA normalization function, ensuring that the final spectral output remains well-conditioned and suitable for high-resolution radar imaging.

The final super-resolved spectral estimate is obtained through an element-wise multiplication of the outputs from the top and bottom networks, directly aligning with the IAA formulation. This structured integration ensures that SR-SPECNet adheres to a model-driven approach rather than relying solely on data-driven learning. The top network captures global dependencies, emulates the inverse covariance transformation, and performs dimensional expansion. Simultaneously, the bottom network stabilizes the spectral estimate, refines local structures, and mitigates sidelobes, collectively enhancing resolution and improving spectral clarity.

C. Data Preprocessing

Proper data normalization is crucial for training neural networks, especially for regression tasks. Different from simulated signals with controlled factors like SNRs, target reflection coefficients, and target number, real-world signals add unpredictability in SNR and reflection coefficients, challenging normalization. SNR varies significantly within a radar frame and from frame to frame. Maintaining a comparable intensity among beam vectors is crucial for constructing accurate RA heatmaps. We introduce a frequency domain normalization method designed to produce consistent and interpretable inputs for neural network training. This approach entails determining a normalization factor, α, for each beam vector, calculated as the maximum absolute value of the frequency spectra, obtained by multiplying $\mathbf{A}^H$ to the beam vector, equivalent to an FFT operation, and then divided by the total number of elements, N_{ch}:

$$\alpha = \max\left(\left|\frac{\mathbf{A}^H(\boldsymbol{\theta})\mathbf{y}}{N_{\text{ch}}}\right|\right). \tag{10}$$

Subsequently, the raw signal $\mathbf{y}$ is normalized using α to yield $\mathbf{y}_{\text{norm}} = \mathbf{y}/\alpha$, ensuring that the signal levels are stable across varying SNR conditions. Similarly, the label, represented by the IAA spectra $\hat{\mathbf{s}}_{\text{IAA}}$, is normalized to $\mathbf{s}_{\text{norm}} = \hat{\mathbf{s}}_{\text{IAA}}/\alpha$. This normalization strategy effectively scales the signal and the IAA spectra so that their values fall within a comparable range, thereby facilitating more effective network training.

Moreover, α preserves the relative intensity across all beam vectors in a radar frame, maintaining the spatial relationships essential for accurate synthesis of RA heatmaps.

D. Signal Level Augmentation

Data augmentation, crucial for enhancing deep learning model robustness and preventing overfitting, is implemented by artificially expanding the dataset with transformations such as flipping, rotation, and translation [64]. While these techniques are well-established in the realm of image processing, the domain of radar signal processing conspicuously lacks bespoke augmentation methods. Addressing this gap, we introduce a novel approach tailored specifically for radar signal augmentation. This method aims to enrich the training dataset, thereby improving the generalization capability of models dedicated to processing radar signals.

1) Flip: Unlike the flip augmentation applied to images, flipping the spectrum in radar signal processing involves taking the complex conjugate of the signal. This process changes the sign of the imaginary part of the signal's complex representation, effectively mirroring the spectral components.

2) Shift: In contrast to the simple circular shift utilized in image augmentation, frequency shifting in signal processing adopts a more sophisticated approach. This technique involves modulating the signal by element-wise multiplying the signal vector $\mathbf{y}$ with the array response vector $\mathbf{a}(\Delta\theta)$, where $\Delta\theta$ represents the angle of shift. The resulting operation is articulated in the following equation:

$$\mathbf{y}_{\text{shift}} = \mathbf{a}(\Delta\theta) \odot \mathbf{y}, \tag{11}$$

where $\odot$ denotes the element-wise multiplication. This modulation effectively shifts the signal's spectrum, thereby facilitating the desired augmentation.

E. SNR-Guided Loss Function

The normalization factor α, representing the maximum value in the signal's frequency domain, is directly proportional to the signal's SNR. A higher α indicates a higher SNR, which in turn suggests a more significant impact on the quality of the final RA heatmap. We propose a novel loss function that prioritizes signals with higher SNRs during the training process. This SNR-guided loss function is designed to emphasize the importance of high-quality signals, ensuring that the model focuses on learning from the most informative data points. By incorporating the SNR information into the

loss calculation, we effectively assign higher weights to signals with better SNRs, akin to a weighted mean squared error (MSE) approach. The loss function is defined as follows:

$$\mathcal{L}_{\text{SNR}} = \alpha \cdot \frac{1}{L} \sum_{i=1}^{L} (s_i - \hat{s}_i)^2, \tag{12}$$

where L is the number of samples, s_i is the actual value, and $\hat{s}_i$ is the predicted value for each sample. This approach ensures that our model is finely tuned to emphasize higher quality signals.

IV. Experiment

We trained and evaluated our SR-SPECNet model using our own dataset of $17,000$ frames of raw ADC radar data. To enhance data diversity and reduce redundancy from consecutive frames, we strategically selected every tenth frame, resulting in a subset of $1,700$ frames. Of these, the first $1,400$ frames were used for training, while the remaining 300 frames were reserved for testing. To further assess the generalizability of our proposed methods, we utilized raw data from the Radartron dataset [48]. Applying the same signal processing steps on the Radartron dataset, we generated an additional $2,667$ frames for testing. It is noteworthy that while Radartron uses the same TI cascade radar board for data collection, it employs different radar parameters, providing an excellent opportunity to evaluate the methods' generalizability.

A. Benchmarks

To assess the effectiveness of SR-SPECNet, we compare it against leading models in line spectrum estimation and high-resolution imaging. Specifically, for line spectrum estimation, we selected the DeepFreq network [37] and SDOA-Net [36], both of which are tailored for learning signal frequency representations for DOA estimation, serving as pertinent benchmarks. Additionally, our evaluation encompasses models that enhance spatial resolution, such as the 2D U-Net [63], which converts low-resolution RA heatmaps to high-resolution equivalents, and the 3D U-Net [23], designed to improve low-resolution Range-Azimuth-Doppler (RAD) data into detailed high-resolution RAD data cube.

B. Evaluation Metrics

We utilize MSE and mean absolute error (MAE) as our primary metrics to assess the effectiveness of our approach in 1D line spectra estimation. To comprehensively assess the quality of the high-resolution RA heatmaps, we employ established image evaluation metrics. Specifically, we use normalized mean squared error (NMSE) to quantify the magnitude of errors, peak signal-to-noise ratio (PSNR) in decibels (dB) to measure the ratio of signal power to noise power affecting image fidelity, and the structural similarity index (SSIM) to evaluate changes in image composition that impact perceived quality. Collectively, these metrics provide a robust assessment.

C. Implementation Details

The task of super-resolution RA heatmap is framed as a 1D line spectra estimation problem, utilizing beam vectors as input data. Our radar configuration involves $N_{\text{fast}} = 256$ fast-time samples, $N_{\text{slow}} = 64$ slow-time samples, and post-MIMO processing, yielding beam vectors with 86 elements each. This configuration results in a raw radar ADC data cube $I_{\text{ADC}} \in \mathbb{C}^{256\times64\times86}$, as depicted in Fig 3. After applying a Range-Doppler FFT, we obtain the Range-Doppler-Channel data $I_{\text{RDC}} \in \mathbb{C}^{256\times64\times86}$. For efficiency and to reduce memory requirements during training, we truncate I_{RDC} along the range axis to the first 200 elements and along the channel axis to the first 10 elements, resulting in a truncated dataset $I_{\text{RDC}}^{\text{trunc}} \in \mathbb{C}^{200\times64\times10}$.

We set the angular grid size to $L = 256$ for frequency domain uniformity. The labels for our 10-element antenna arrays are derived from the IAA spectra of a 20-element antenna array to achieve higher resolution spectra.

As shown in Fig 4, the input to SR-SPECNet, beam vector $\mathbf{y}_1 \in \mathbb{C}^{10}$, is processed using a 10-element DBF to obtain the initial estimated spectra $\hat{\mathbf{S}}_{(0)} \in \mathbb{R}^{256}$. This is input into a 1D U-Net consisting of four down-sampling and four up-sampling layers, with channel sizes for the down-sampling layers set at 16, 32, 64, and 128, and for the up-sampling layers at 64, 32, 16, and 8, culminating in an output layer with a channel size of one. The final output of the 1D U-Net matches the size of $\hat{\mathbf{S}}_{(0)}$. Concurrently, $\hat{\mathbf{S}}_{(0)}$ is concatenated with the processed beam vector, split into real and imaginary parts, to form an input to the MLP network of size 276. The MLP network consists of four fully connected layers with output sizes of 1024, 512, 256, and 40. Each layer is followed by a ReLU activation layer, except for the last layer. The MLP output is transformed into a complex number by using the first 20 numbers as the real part and the last 20 as the imaginary part, creating the estimated beam vector $\hat{\mathbf{y}}_2$ for a 20-element antenna array. This is followed by a 20-element DBF, ensuring that the output sizes of both network sections match. An element-wise multiplication is then applied to produce the final estimated spectra $\hat{\mathbf{S}}$.

SR-SPECNet and the benchmark models were implemented using PyTorch, with training standardized using the Adam optimizer at a learning rate of 0.0001 for 500 epochs, accelerated on four Nvidia RTX A6000 GPUs for efficiency.

D. Results and Comparisons in Super-Resolution

1) Spectra Estimation: We benchmarked the performance of our SR-SPECNet against two established one-dimensional baseline models, as detailed in IV-A. For consistency, each model was trained using an MSE loss function. All models were trained under two scenarios, with and without signal-level augmentation, to demonstrate the effectiveness of our proposed augmentation method. The results, detailed in Table II, reveal distinct performance characteristics. Notably, SR-SPECNet outperforms the baseline models, achieving the lowest MSE and MAE in both scenarios.

A closer examination of Table II shows that the DeepFreq model [37] has the fewest trainable parameters, while SDOA-

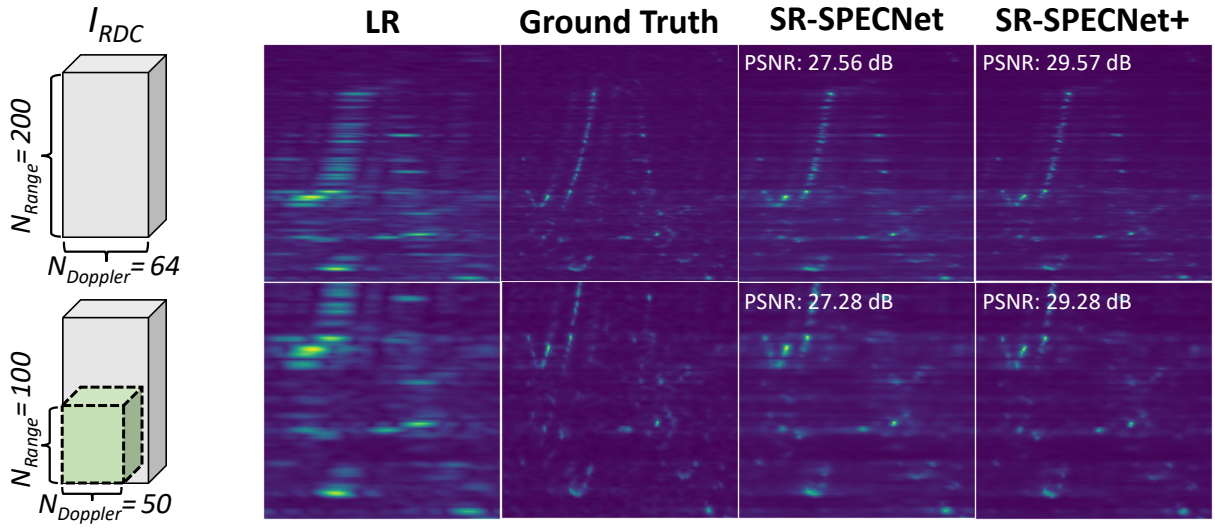

Figure 5: Scalability of SR-SPECNet and SR-SPECNet+ across variable N_{Range} and N_{Doppler}. The figure contrasts RA heatmap reconstructions using SR-SPECNet and SR-SPECNet+, respectively. In the first row, $N_{\text{Range}} = 200$, $N_{\text{Doppler}} = 64$; in the second row, $N_{\text{Range}} = 10$, $N_{\text{Doppler}} = 50$, showcasing the model's scalability.

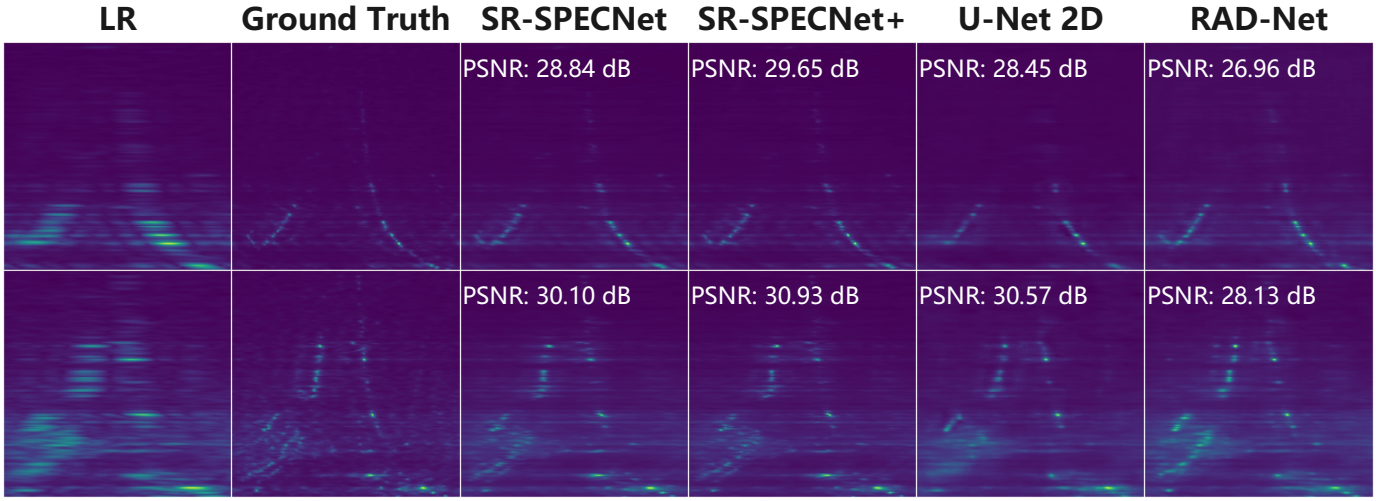

Figure 6: RA heatmap quality comparison. Heatmaps from the same radar frame are reconstructed by SR-SPECNet, SR-SPECNet+, and baseline 2D U-Net and 3D RAD-Net models, alongside the ground truth.

Net [36] has the most. Surprisingly, despite SDOA-Net's increased complexity and higher number of parameters, it fails to provide a significant performance boost over DeepFreq. In contrast, our SR-SPECNet, which contains 1.1205 million parameters, substantially fewer than SDOA-Net, achieves the best performance among the three models. Without signal-level augmentation, SR-SPECNet attains an MSE of 0.0072 and an MAE of 0.0488. When signal-level augmentation is applied, the performance is further enhanced to an MSE of 0.0065 and an MAE of 0.0459.

2) Single-Target DOA Estimation Accuracy: To evaluate the accuracy of SR-SPECNet in estimating the DOA for a single target, we conducted a Monte Carlo simulation with $2,000$ trials for each SNR level, ranging from 0 dB to 30 dB in 5 dB increments. The root mean squared error (RMSE) of the DOA estimation was computed for each SNR level and compared against baseline methods, including model-based algorithms such as FFT and IAA, deep learning networks like DeepFreq and SDOA-Net, and the Cramer-Rao lower bound (CRLB). The results are shown in Figure 7, with the black dashed line representing the grid-induced error.

SR-SPECNet outperforms the benchmark deep learning networks across all SNR levels. At 0 dB, it achieves the best performance among all methods, including FFT and IAA. From 5 dB to 15 dB, SR-SPECNet demonstrates comparable accuracy to FFT and IAA, highlighting its robustness in low to moderate SNR scenarios. At higher SNR levels, specifically between 20 dB and 30 dB, the performance of SR-SPECNet shows a slight decline relative to IAA and FFT. This behavior can be explained by the distribution of training data: the

Models	P(M)	w/o Augmentation		w Augmentation	
		MSE↓	MAE↓	MSE↓	MAE↓
DeepFreq [37]	0.0232	0.0103	0.0613	0.0100	0.0598
SDOA-Net [36]	5.3050	0.0104	0.0603	0.0099	0.0593
SR-SPECNet	1.1205	**0.0072**	**0.0488**	**0.0065**	**0.0459**

Table II: Comparative performance metrics for different deep learning models. MSE and MAE are reported alongside the number of parameters (P) in millions (M).

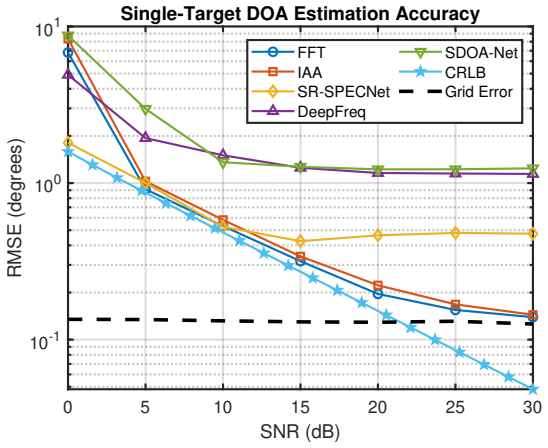

Figure 7: RMSE of DOA estimation for SR-SPECNet, FFT, IAA, SDOA-Net, DeepFreq, and the CRLB across SNR levels, with the black dashed line indicating the grid-induced error.

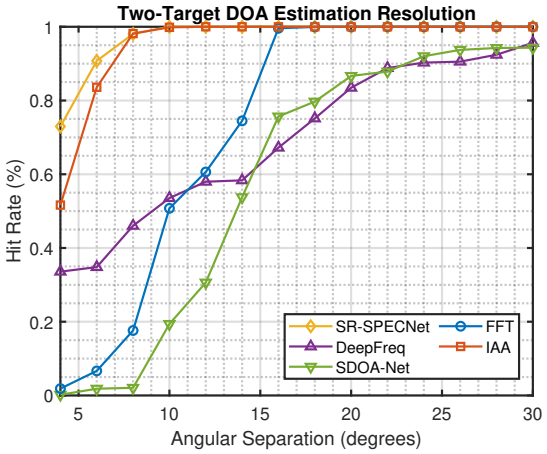

Figure 8: Hit rate as a function of angular separation ($\Delta\theta$) for two closely spaced targets at an SNR of 15 dB. The performance of SR-SPECNet, FFT, IAA, DeepFreq, and SDOA-Net is compared. A trial is considered successful if both targets are correctly detected and resolved.

real-world radar dataset used to train SR-SPECNet contains fewer high-SNR samples, as such conditions are less common in practical automotive radar scenarios. Consequently, the network is less exposed to high-SNR data during training, which limits its ability to achieve optimal performance in these regimes. In contrast, IAA and FFT are not influenced by data limitations and consistently perform well across all SNR levels.

3) Resolution of Closely Spaced Targets: To evaluate the resolution capability of SR-SPECNet and benchmark methods, a Monte Carlo simulation was conducted with two closely spaced targets at an SNR of 15 dB. The angular separation ($\Delta\theta$) between the targets was varied from 4° to 30° in steps of 2°. For each angular separation, $2,000$ trials were performed. A trial was considered successful if both targets were correctly detected and resolved, defined as the angular estimation error for each target being smaller than 1°. The hit rate was calculated as the ratio of successful trials to the total number of trials and is presented as a function of $\Delta\theta$ in Figure 8.

As shown in Figure 8, SR-SPECNet demonstrates superior resolution capability compared to DeepFreq and SDOA-Net, particularly for smaller angular separations. Below 10°, SR-SPECNet achieves higher hit rates than IAA, while at 10° and above, both SR-SPECNet and IAA resolve all targets in every trial. These results highlight SR-SPECNet's ability to effectively resolve closely spaced targets.

4) High-Resolution RA Heatmap: We subsequently investigated the performance of deep learning networks in generating high-resolution RA heatmaps. To this end, we evaluated SR-SPECNet and SR-SPECNet+, trained using MSE loss and our novel SNR-guided loss, respectively, against established benchmark models. As detailed in Table III, our models were tested on both our own dataset and the Radartron dataset [48].

SR-SPECNet is specifically designed for one-dimensional line spectra estimation and consequently has significantly fewer parameters and lower model complexity compared to the 2D U-Net (31.0365 million parameters) and the 3D RAD-Net (56.4639 million parameters). Despite its lower complexity, SR-SPECNet demonstrates strong performance, as evidenced in Table III.

To ensure fair evaluation across datasets, we use NMSE instead of MSE, as it normalizes errors relative to the total magnitude of the ground truth, making it more robust to variations in target density and radar configurations. In our self-built dataset, which captures long-range scenes, the ground truth often contains extensive regions with low-magnitude values, resulting in a smaller overall sum of squared values. As a result, even minor prediction errors appear disproportionately large when normalized in NMSE. This effect is less pronounced in the Radartron dataset, where targets are more densely distributed. Despite this, SR-SPECNet maintains consistent NMSE performance, demonstrating its robustness

	Models	P(M)	Ours			Radatron [48]		
			NMSE↓	SSIM↑	PSNR↑	NMSE↓	SSIM↑	PSNR↑
2D	U-Net [63]	31.0365	1.3577	0.7795	30.0893	0.4674	0.7083	24.6722
3D	RAD-Net [23]	56.4639	2.1679	0.7215	28.5328	0.6001	0.6915	24.9197
1D	SR-SPECNet	1.1205	0.4026	0.8560	31.4797	0.2724	0.7535	25.7391
	SR-SPECNet+		**0.1543**	**0.9149**	**36.6608**	**0.1697**	**0.7746**	**28.2755**

Table III: Performance metrics of deep learning models for super-resolution RA heatmap generation.

across different radar conditions.

The proposed SR-SPECNet demonstrates consistent performance across both datasets, as reflected in NMSE, SSIM, and PSNR metrics, highlighting its robustness in handling variations in radar configurations and driving scenarios. The key advantage of SR-SPECNet lies in its 1D spectral estimation approach, which extracts signal features that remain invariant across different radar setups and environments. In contrast, 2D and 3D methods depend on spatial features that are significantly affected by variations in radar configuration, such as range resolution (determined by radar bandwidth), Doppler resolution, maximum detectable range, and other system-dependent factors, as well as changes in target distribution due to different driving scenarios. These dependencies can lead to feature shifts in the 2D and 3D domains, reducing their generalizability across datasets. SR-SPECNet, however, maintains stable spectral features, avoiding these challenges and ensuring consistent performance. It consistently outperforms the 2D U-Net on both our dataset and the Radartron dataset, demonstrating superior generalizability. This underscores the advantage of generating RA heatmaps through 1D spectral estimation, as well as the impact of domain-specific enhancements in SR-SPECNet+, which further strengthen its performance. By incorporating an SNR-guided loss function, SR-SPECNet+ effectively fine-tunes the training process to emphasize signals with higher SNR, leading to improved spectral estimation. As a result, SR-SPECNet+ emerges as the leading model, outperforming both the 2D U-Net and 3D RAD-Net benchmarks, as well as SR-SPECNet, on both datasets, achieving the lowest NMSE and the highest SSIM and PSNR scores.

5) Scalability: Unlike the 2D U-Net and 3D RAD-Net models that require inputs of fixed dimensions, the 2D U-Net processes low-resolution RA heatmaps and the 3D RAD-Net handles low-resolution RAD data, our SR-SPECNet model is designed for adaptability by accepting 1D beam vectors as input. This flexibility grants SR-SPECNet superior scalability across varying N_{Range} and N_{Doppler} values.

Figure 5 illustrates the performance of SR-SPECNet and SR-SPECNet+ with varying input dimensions. In the first row, the original Range-Doppler-Channel data I_{RDC} has dimensions $N_{\text{Range}} = 200$ and $N_{\text{Doppler}} = 64$, as used for training (see Section IV-C). Under these settings, both networks generate high-resolution RA maps with PSNR values of 27.56 dB and 29.57 dB, respectively. In the second row of Figure 5, the dimensions of I_{RDC} are reduced to $N_{\text{Range}} = 100$ and $N_{\text{Doppler}} = 50$. Remarkably, both SR-SPECNet and SR-SPECNet+ adapt seamlessly to these new sizes without significant loss in PSNR, demonstrating their robustness and flexibility to accommodate different N_{Range} and N_{Doppler} values.

Moreover, as 4D automotive radars, which encompass range, Doppler, azimuth, and elevation dimensions, gain increasing attention from both industry and academia, the scalability of our approach becomes even more valuable. Traditional methods like employing a 4D U-Net to enhance radar resolution significantly increase the number of parameters and computational complexity. In contrast, SR-SPECNet and SR-SPECNet+ efficiently handle higher-dimensional data without a substantial rise in complexity, making them more practical for advancing 4D radar technologies.

6) Dynamic Range: In automotive radar sensing, reflections vary in intensity, with strong targets producing returns with high amplitudes and weak targets exhibiting lower amplitudes. A key concern is whether SNR-guided loss, which prioritizes high-SNR regions, impacts weak target imaging. To assess this, we evaluate model performance across different dynamic ranges.

We define dynamic range as the ratio (in dB) between the peak amplitude of the entire image and the peak amplitude within a selected small region in the far field, where the target reflections are typically weaker. This metric quantifies the disparity between strong and weak scatterers, providing insight into a model's ability to preserve weaker target information in varying scenarios.

The results, summarized in Table IV, show that SR-SPECNet+ demonstrates strong performance across most metrics and dynamic range categories due to its strong ability to suppress target sidelobes, particularly excelling in NMSE and PSNR. For low dynamic range images, SR-SPECNet+ achieves the best results in all metrics, effectively preserving weak target imaging. In medium and high dynamic ranges, it maintains superior NMSE and PSNR performance, showcasing robustness in handling significant power variations. While SR-SPECNet achieves slightly higher SSIM scores in medium and high dynamic ranges, SR-SPECNet+ strikes a better overall balance across all metrics, ensuring reliable reconstruction of both strong and weak targets.

7) Ablation Study: To better evaluate the performance impact of data augmentation and the SNR-guided loss function, we conduct a systematic ablation study on SR-SPECNet and two baseline models. These experiments aim to assess the independent contributions of these components and validate their generalization capability across different network architectures.

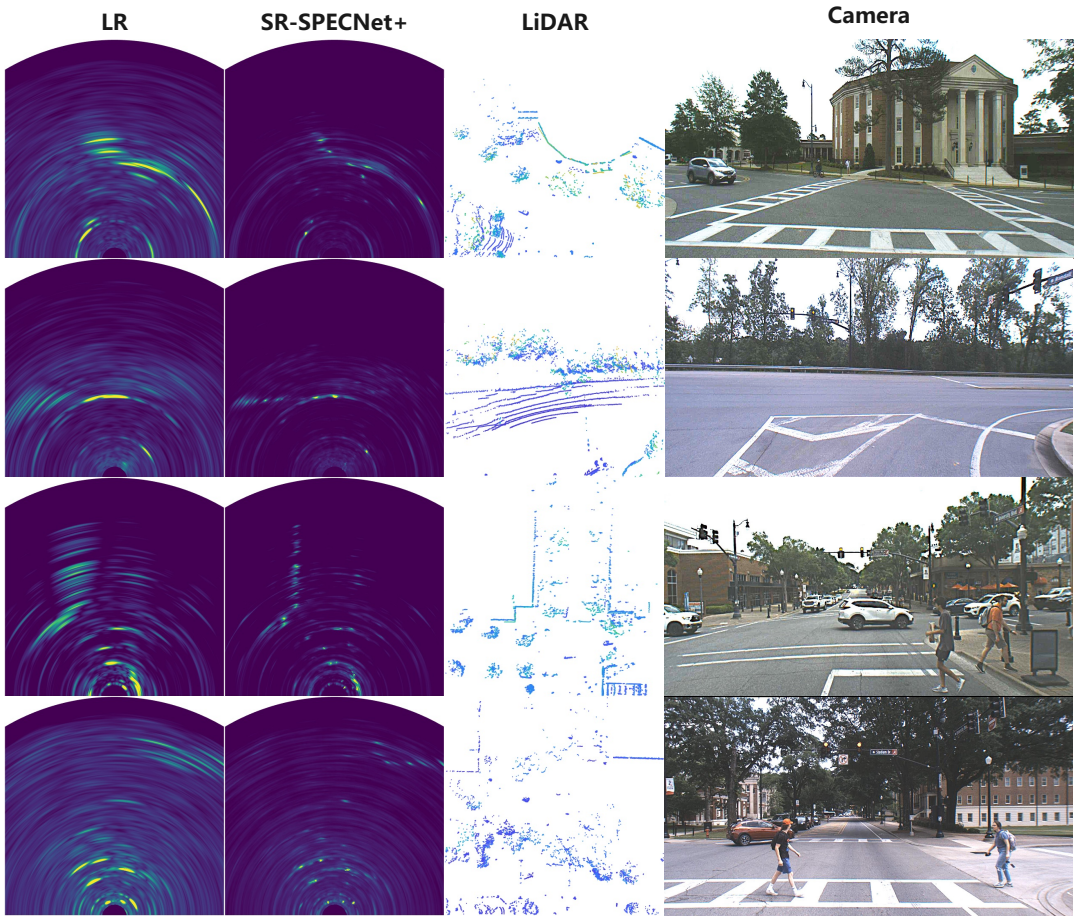

Figure 9: BEV heatmap quality comparison. Low-resolution radar BEVs alongside high-resolution radar BEVs generated by SR-SPECNet+. Corresponding LiDAR point clouds and camera images are included for reference, demonstrating the enhanced resolution achieved by our method.

	Models	Low			Medium			High		
		NMSE↓	SSIM↑	PSNR↑	NMSE↓	SSIM↑	PSNR↑	NMSE↓	SSIM↑	PSNR↑
2D	U-Net [63]	0.4145	0.4936	16.3978	0.4191	0.4953	16.4779	0.4433	0.5003	16.4683
3D	RAD-Net [23]	0.3423	0.5229	17.8972	0.4241	0.5261	17.5499	0.4278	0.5278	17.4540
1D	SR-SPECNet	0.1881	0.5835	19.3013	0.2031	**0.6001**	19.3316	0.1938	**0.5971**	19.1722
	SR-SPECNet+	**0.1272**	**0.5923**	**21.1618**	**0.1118**	0.5827	**20.7491**	**0.0941**	0.5180	**19.5597**

Table IV: Model performance across different dynamic ranges. The test dataset is divided into three groups: low dynamic range (2 dB - 10 dB, 790 images), medium dynamic range (10 dB - 20 dB, 821 images), and high dynamic range ($>$ 20 dB, 544 images). While a 20 dB dynamic range may not seem high, it represents the peak value within the test image. These images still contain smaller-magnitude scatterers, making it a relevant benchmark for assessing weak target imaging performance. NMSE, SSIM, and PSNR are evaluated to measure each model's ability to reconstruct weak targets.

Models	Ablation Settings		NMSE↓	SSIM↑	PSNR↑
	SA	SGL			
SR-SPECNet	✗	✗	0.3123	0.7291	26.9376
	✓	✗	0.2867	0.7648	26.3695
	✗	✓	0.2625	0.7738	27.3694
	✓	✓	**0.1680**	**0.7901**	**29.1963**
DeepFreq [37]	✗	✗	3.9894	0.4955	16.6768
	✓	✗	2.8625	0.5448	19.8862
	✗	✓	0.5766	0.6956	24.1084
	✓	✓	**0.3388**	**0.7318**	**26.1257**
SDOA-Net [36]	✗	✗	2.7024	0.5340	18.9596
	✓	✗	1.7460	0.5967	21.1684
	✗	✓	0.5218	0.7031	24.8092
	✓	✓	**0.3144**	**0.7545**	**26.6423**

Table V: Ablation study results evaluating the impact of signal level augmentation (SA) and the SNR-guided loss (SGL) on SR-SPECNet and two benchmark models. The results show improvements in NMSE, SSIM, and PSNR when both components are included, demonstrating their effectiveness and generalization capability.

The ablation study results in Table V demonstrate the significant impact of signal augmentation and the SNR-guided loss (SGL) function on spectral reconstruction performance. Removing both components results in higher NMSE, lower SSIM, and reduced PSNR across all models, indicating degraded performance. Applying SA improves generalization by introducing signal variations, while SGL enhances spectral estimation by prioritizing high-SNR signals during training. When both techniques are applied together, the largest gains are observed, with SR-SPECNet achieving the best performance, reducing NMSE from 0.3123 to 0.1680 and improving SSIM and PSNR to 0.7901 and 29.1963 dB, respectively. Similar trends in DeepFreq and SDOA-Net confirm that these enhancements generalize beyond SR-SPECNet. This study validates the effectiveness of the proposed methods in improving spectral estimation, robustness, and generalization across different network architectures.

8) Complexity: To evaluate the complexity of the proposed SR-SPECNet compared to benchmark networks and IAA, we use three key metrics: the number of trainable parameters, peak memory usage, and inference time. The inference time is measured as the average time required to generate one radar range-angle (RA) map. It is worth noting that faster variations of IAA, such as fast IAA (FIAA) [65] and super fast IAA (SFIAA) [66], replace the covariance matrix inversion with matrix factorization to reduce computational cost. However, their speed advantage is minimal for small arrays (e.g., a 10-element array, as in our setup). Consequently, they do not significantly impact inference time in our experiments and are omitted from the comparative table.

The computational complexity of SR-SPECNet is evaluated against other benchmark networks, including IAA. SR-SPECNet achieves a balanced trade-off between efficiency and performance, with 1.1205 million trainable parameters, 418.33 MB peak memory usage, and a 5.75 ms inference time. Compared to deep learning methods, SR-SPECNet is significantly more efficient than U-Net (31.0365M parameters, 468.09 MB, 5.41 ms) and RAD-Net (56.4639M parameters, $1,809.48$ MB, 6.87 ms). While DeepFreq is lightweight (0.0232M parameters, 151.82 MB, 1.22 ms), its limited model capacity may hinder performance on complex tasks.

In contrast, IAA, while capable of generating super-resolution spectra for a 10-element ULA, is impractical due to its excessive memory usage ($1,0261.84$ MB) and slow inference time (356.79 ms). It is important to note that all deep learning networks, including SR-SPECNet, are trained to generate spectra for a 20-element ULA, providing higher resolution. This highlights the advantage of deep learning over traditional methods like IAA.

E. Visualization of RA maps

To evaluate the quality of the high resolution RA heatmaps produced by SR-SPECNet and SR-SPECNet+, we visually compare their outputs against those from baseline models, namely 2D U-Net and 3D RAD-Net, as depicted in Figure 6. The low resolution (LR) heatmaps are generated using FFT with a 10-element antenna arrays, while the ground truth heatmaps are generated using the IAA method with a 20-element antenna arrays. Due to the larger antenna aperture size and the application of super-resolution algorithm, these ground truth heatmaps have much better resolution than the LR heatmap. Furthermore, IAA suppresses sidelobes, yielding much clearer heatmaps. This underscores the benefits of using IAA derived heatmaps as ground truth for learning, rather than relying on FFT-generated heatmaps with a larger antenna aperture, which may not always be practically available due to hardware costs and the complexities involved in MIMO technology implementations.

Fig. 6 demonstrates that the RA heatmaps that are respectively produced by SR-SPECNet and SR-SPECNet+ with a SNR-guided loss function, exhibit a noticeable improvement over the heatmaps generated by baseline models, aligning with the quantitative metrics presented in Tables III. These results collectively affirm the effectiveness of our proposed 1D methodologies over the 2D and 3D methods.

To further demonstrate the efficacy of our approach in enhancing RA heatmap resolution, we convert the RA heatmaps from polar to Cartesian coordinates, resulting in bird's eye views (BEVs). Figure 9 displays low-resolution BEVs and high-resolution BEVs generated by SR-SPECNet+, alongside their corresponding LiDAR point clouds and camera images. The results clearly show that our method significantly enhances the resolution.

V. Conclusion

In this paper, we tackled the limitations of mmWave radar imaging for autonomous vehicle perception, specifically addressing the issue of insufficient spatial resolution for precise semantic scene interpretation. Recognizing that traditional

Models		P (M)	Memory Usage (MB)	Inference Time (ms)
2D	U-Net [63]	31.0365	468.09	5.41
3D	RAD-Net [23]	56.4639	1809.48	6.87
1D	DeepFreq [37]	0.0232	151.82	1.22
	SDOA-Net [36]	5.3050	6522.57	1.83
	SR-SPECNet	1.1205	418.33	5.75
	IAA [19]	-	10261.84	356.79

Table VI: Comparison of model complexity metrics, including the number of trainable parameters (P), peak memory usage, and inference time for processing one radar frame.

super-resolution techniques from optical imaging do not adequately capture the unique characteristics of radar signal data, we redefined radar imaging super-resolution as a one-dimensional signal super-resolution spectra estimation problem. By leveraging radar signal processing domain knowledge, we introduced innovative methods such as data normalization, signal-level augmentation, and a domain-informed SNR-guided loss function. Our proposed deep learning network, SR-SPECNet, is specifically tailored for automotive radar imaging and demonstrates remarkable scalability, parameter efficiency. Extensive testing confirms that SR-SPECNet sets a new benchmark in producing high-resolution radar range-azimuth images, significantly enhancing radar imaging quality and resolution compared to existing methods.

Additionally, we presented a novel real-world radar dataset that is crucial for advancing radar imaging techniques and refining super-resolution spectra estimation methods. This dataset, along with our source code, will be made publicly available to foster further research in this domain. In summary, our work offers a comprehensive solution to enhance mmWave radar imaging for autonomous vehicles, effectively bridging the gap between radar signal processing and deep learning. By redefining the super-resolution problem and introducing domain-specific innovations, we provide a pathway towards more accurate and reliable perception systems in autonomous vehicles. Future work may explore extending these methodologies to other radar modalities and further optimizing the network for real-time applications.

REFERENCES

[1] S. Patole, M. Torlak, D. Wang, and M. Ali, "Automotive radars: A review of signal processing techniques," *IEEE Signal Processing Magazine*, vol. 34, no. 2, pp. 22–35, 2017.

[2] F. Engels, P. Heidenreich, A. M. Zoubir, F. K. Jondral, and M. Wintermantel, "Advances in automotive radar: A framework on computationally efficient high-resolution frequency estimation," *IEEE Signal Processing Magazine*, vol. 34, no. 2, pp. 36–46, 2017.

[3] S. Sun, A. P. Petropulu, and H. V. Poor, "MIMO radar for advanced driver-assistance systems and autonomous driving: Advantages and challenges," *IEEE Signal Processing Magazine*, vol. 37, no. 4, pp. 98–117, 2020.

[4] C. Waldschmidt, J. Hasch, and W. Menzel, "Automotive radar - From first efforts to future systems," *IEEE Journal of Microwaves*, vol. 1, no. 1, pp. 135–148, 2021.

[5] M. Markel, *Radar for Fully Autonomous Driving*. Boston, MA: Artech House, 2022.

[6] Z. Peng, C. Li, and F. Uysal, *Modern Radar for Automotive Applications*. London, UK: IET, 2022.

[7] R. Zheng, S. Sun, H. Liu, and T. Wu, "Deep-neural-network-enabled vehicle detection using high-resolution automotive radar imaging," *IEEE Transactions on Aerospace and Electronic Systems*, vol. 59, no. 5, pp. 4815–4830, 2023.

[8] L. Xu, R. Zheng, and S. Sun, "A deep reinforcement learning approach for integrated automotive radar sensing and communication," in *2022 IEEE 12th Sensor Array and Multichannel Signal Processing Workshop (SAM)*. IEEE, 2022, pp. 316–320.

[9] L. Xu, S. Sun, K. V. Mishra, and Y. D. Zhang, "Automotive FMCW radar with difference co-chirps," *IEEE Transactions on Aerospace and Electronic Systems*, vol. 59, no. 6, pp. 8145–8165, 2023.

[10] S. Sun and Y. D. Zhang, "4D automotive radar sensing for autonomous vehicles: A sparsity-oriented approach," *IEEE Journal of Selected Topics in Signal Processing*, vol. 15, no. 4, pp. 879–891, 2021.

[11] G. Duggal, S. Vishwakarma, K. V. Mishra, and S. S. Ram, "Doppler-resilient 802.11ad-based ultrashort range automotive joint radar-communications system," *IEEE Transactions on Aerospace and Electronic Systems*, vol. 56, no. 5, pp. 4035–4048, 2020.

[12] F. Engels, P. Heidenreich, M. Wintermantel, L. Stäcker, M. Al Kadi, and A. M. Zoubir, "Automotive radar signal processing: Research directions and practical challenges," *IEEE Journal of Selected Topics in Signal Processing*, vol. 15, no. 4, pp. 865–878, 2021.

[13] J. Li and P. Stoica, "MIMO radar with colocated antennas," *IEEE Signal Processing Magazine*, vol. 24, no. 5, pp. 106–114, 2007.

[14] ——, *MIMO Radar Signal Processing*. Hoboken, NJ, Wiley, 2009.

[15] J. Bergin and J. R. Guerci, *MIMO Radar: Theory and Application*. Boston, MA, Artech House, 2018.

[16] D. L. Donoho, "Compressed sensing," *IEEE Transactions on Information Theory*, vol. 52, no. 4, pp. 1289–1306, 2006.

[17] E. Candès and J. Romberg, "Sparsity and incoherence in compressive sampling," *Inverse problems*, vol. 23, no. 3, p. 969, 2007.

[18] E. Candes and C. Fernandez-Granda, "Towards a mathematical theory of super-resolution," *Communications on Pure and Applied Mathematics*, vol. 67, no. 6, pp. 906–956, 2014.

[19] T. Yardibi, J. Li, P. Stoica, M. Xue, and A. Baggeroer, "Source localization and sensing: A nonparametric iterative adaptive approach based on weighted least squares," vol. 46, no. 1, pp. 425–443, 2010.

[20] W. Roberts, P. Stoica, J. Li, T. Yardibi, and F. Sadjadi, "Iterative adaptive approaches to MIMO radar imaging," vol. 4, no. 1, pp. 5–20, 2010.

[21] K. Armanious, S. Abdulatif, F. Aziz, U. Schneider, and B. Yang, "An adversarial super-resolution remedy for radar design trade-offs," in *2019 27th European Signal Processing Conference (EUSIPCO)*, 2019, pp. 1–5.

[22] A. Geiss and J. C. Hardin, "Radar super resolution using a deep convolutional neural network," *Journal of Atmospheric and Oceanic Technology*, vol. 37, no. 12, pp. 2197–2207, 2020.

[23] Y.-J. Li, S. Hunt, J. Park, M. O'Toole, and K. Kitani, "Azimuth super-resolution for FMCW radar in autonomous driving," in *Proceedings of the IEEE/CVF Conference on Computer Vision and Pattern Recognition (CVPR)*, 2023, pp. 17 504–17 513.

[24] H. Krim and M. Viberg, "Two decades of array signal processing research: the parametric approach," *IEEE Signal Processing Magazine*, vol. 13, no. 4, pp. 67–94, 1996.

[25] M. Pesavento, M. Trinh-Hoang, and M. Viberg, "Three more decades in array signal processing research: An optimization and structure exploitation perspective," *IEEE Signal Processing Magazine*, vol. 40, no. 4, pp. 92–106, 2023.

[26] M. A. Richards, *Fundamentals of Radar Signal Processing, 3rd Ed*. New York, McGraw-Hill, 2022.

[27] R. O. Schmidt, *A signal subspace approach to multiple emitter location and spectral estimation*. Stanford University, 1982.

[28] R. Roy and T. Kailath, "ESPRIT-estimation of signal parameters via rotational invariance techniques," *IEEE Transactions on Acoustics, Speech, and Signal Processing*, vol. 37, no. 7, pp. 984–995, 1989.
[29] G.-O. Glentis and A. Jakobsson, "Efficient implementation of iterative adaptive approach spectral estimation techniques," *IEEE Transactions on Signal Processing*, vol. 59, no. 9, pp. 4154–4167, 2011.
[30] M. Xue, L. Xu, and J. Li, "IAA spectral estimation: Fast implementation using the Gohberg-Semencul factorization," *IEEE Transactions on Signal Processing*, vol. 59, no. 7, pp. 3251–3261, 2011.
[31] G. O. Glentis and A. Jakobsson, "Superfast approximative implementation of the IAA spectral estimate," *IEEE Transactions on Signal Processing*, vol. 60, no. 1, pp. 472–478, 2012.
[32] G. K. Papageorgiou, M. Sellathurai, and Y. C. Eldar, "Deep networks for direction-of-arrival estimation in low snr," *IEEE Transactions on Signal Processing*, vol. 69, pp. 3714–3729, 2021.
[33] J. Fuchs, M. Gardill, M. Lübke, A. Dubey, and F. Lurz, "A machine learning perspective on automotive radar direction of arrival estimation," *IEEE Access*, vol. 10, pp. 6775–6797, 2022.
[34] S. Feintuch, J. Tabrikian, I. Bilik, and H. H. Permuter, "Neural network-based DOA estimation in the presence of non-Gaussian interference," *arXiv preprint arXiv:2301.02856*, 2023.
[35] M. Gall, M. Gardill, J. Fuchs, and T. Horn, "Learning representations for neural networks applied to spectrum-based direction-of-arrival estimation for automotive radar," in *2020 IEEE/MTT-S International Microwave Symposium (IMS)*. IEEE, 2020, pp. 1031–1034.
[36] P. Chen, Z. Chen, L. Liu, Y. Chen, and X. Wang, "Sdoa-net: An efficient deep learning-based doa estimation network for imperfect array," *IEEE Transactions on Instrumentation and Measurement*, 2024.
[37] G. Izacard, S. Mohan, and C. Fernandez-Granda, "Data-driven estimation of sinusoid frequencies," in *Advances in Neural Information Processing Systems*, vol. 32, 2019.
[38] H. Caesar, V. Bankiti, A. H. Lang, S. Vora, V. E. Liong, Q. Xu, A. Krishnan, Y. Pan, G. Baldan, and O. Beijbom, "nuScenes: A multimodal dataset for autonomous driving," *IEEE/CVF Conference on Computer Vision and Pattern Recognition (CVPR)*, June 16-18, 2020.
[39] D. Barnes, M. Gadd, P. Murcutt, P. Newman, and I. Posner, "The Oxford radar robotcar dataset: A radar extension to the oxford robotcar dataset," in *Proc. IEEE International Conference on Robotics and Automation (ICRA)*, Paris, France, May 31-Oct. 31, 2020.
[40] M. Sheeny, E. D. Pellegrin, M. Saptarshi, A. Ahrabian, S. Wang, and A. Wallace, "RADIATE: A radar dataset for automotive perception," *arXiv preprint arXiv:2010.09076*, 2020.
[41] Y. Wang, Z. Jiang, X. Gao, J.-N. Hwang, G. Xing, and H. Liu, "RODNet: Radar object detection using cross-modal supervision," in *Proc. IEEE/CVF Winter Conference on Applications of Computer Vision (WACV)*, Waikoloa, HI, Jan. 5-9, 2021.
[42] M. Mostajabi, C. M. Wang, D. Ranjan, and G. Hsyu, "High resolution radar dataset for semi-supervised learning of dynamic objects," in *Proc. IEEE/CVF Conference on Computer Vision and Pattern Recognition (CVPR) Workshops*, Seattle, WA, June 14-19, 2020.
[43] A. Ouaknine, A. Newson, J. Rebut, F. Tupin, and P. Perez, "CARRADA dataset: Camera and automotive radar with range-angle-Doppler annotations," in *Proc. 25th International Conference on Pattern Recognition (ICPR)*, Milan, Italy, Jan. 10-15, 2021.
[44] O. Schumann, M. Hahn, N. Scheiner, F. Weishaupt, J. F. Tilly, J. Dickmann, and C. WÄ¶hler, "RadarScenes: A real-world radar point cloud data set for automotive applications," *arXiv preprint arXiv:2104.02493*, 2021.
[45] J. Rebut, A. Ouaknine, W. Malik, and P. Pérez, "Raw high-definition radar for multi-task learning," in *Proceedings of the IEEE/CVF Conference on Computer Vision and Pattern Recognition (CVPR)*, 2022, pp. 17 021–17 030.
[46] A. Palffy, E. Pool, S. Baratam, J. Kooij, and D. Gavrila, "Multi-class road user detection with 3+1D radar in the view-of-Delft dataset," *IEEE Robotics and Automation Letters*, vol. 7, no. 2, pp. 4961–4968, 2022.
[47] D.-H. Paek, S.-H. Kong, and K. T. Wijaya, "K-radar: 4D radar object detection for autonomous driving in various weather conditions," in *Thirty-sixth Conference on Neural Information Processing Systems Datasets and Benchmarks Track*, 2022. [Online]. Available: https://openreview.net/forum?id=W_bsDmzwaZ7
[48] S. Madani, J. Guan, W. Ahmed, S. Gupta, and H. Hassanieh, "Radatron: Accurate detection using multi-resolution cascaded MIMO radar," in *European Conference on Computer Vision (ECCV)*, 2022, pp. 160–178.
[49] N. Shlezinger, J. Whang, Y. C. Eldar, and A. G. Dimakis, "Model-based deep learning," *Proceedings of the IEEE*, vol. 111, no. 5, pp. 465–499, 2023.
[50] A. Shultzman, E. Azar, M. R. Rodrigues, and Y. C. Eldar, "Generalization and estimation error bounds for model-based neural networks," *arXiv preprint arXiv:2304.09802*, 2023.
[51] V. Monga, Y. Li, and Y. C. Eldar, "Algorithm unrolling: Interpretable, efficient deep learning for signal and image processing," *IEEE Signal Processing Magazine*, vol. 38, no. 2, pp. 18–44, 2021.
[52] D. H. Shmuel, J. P. Merkofer, G. Revach, R. J. Van Sloun, and N. Shlezinger, "Deep root music algorithm for data-driven doa estimation," in *ICASSP 2023-2023 IEEE International Conference on Acoustics, Speech and Signal Processing (ICASSP)*. IEEE, 2023, pp. 1–5.
[53] A. M. Elbir, "DeepMUSIC: Multiple signal classification via deep learning," *IEEE Sensors Letters*, vol. 4, no. 4, pp. 1–4, 2020.
[54] X. Wu, X. Yang, X. Jia, and F. Tian, "A gridless doa estimation method based on convolutional neural network with toeplitz prior," *IEEE Signal Processing Letters*, vol. 29, pp. 1247–1251, 2022.
[55] N. Shlezinger, Y. C. Eldar, and S. P. Boyd, "Model-based deep learning: On the intersection of deep learning and optimization," *IEEE Access*, vol. 10, pp. 115 384–115 398, 2022.
[56] S. Chaudhari and J. M. Moura, "Deep beamforming for joint direction of arrival estimation and source detection," in *2022 56th Asilomar Conference on Signals, Systems, and Computers*, 2022, pp. 1403–1407.
[57] R. Zheng, H. Liu, S. Sun, and J. Li, "Deep learning based computationally efficient unrolling IAA for direction-of-arrival estimation," in *European Signal Processing Conference (EUSIPCO)*, Helsinki, Finland, Sept. 4-8, 2023.
[58] R. Zheng, S. Sun, H. Liu, H. Chen, and J. Li, "Interpretable and efficient beamforming-based deep learning for single-snapshot DOA estimation," *IEEE Sensors Journal*, vol. 24, no. 14, pp. 22 096–22 105, 2024.
[59] https://www.zf.com/products/en/cars/products_64255.html.
[60] Texas Instruments, *Design Guide: TIDEP-01012 Imaging Radar Using Cascaded MmWave Sensor Reference Design*, 2020, rev. A. [Online]. Available: https://www.ti.com/lit/ug/tiduen5a/tiduen5a.pdf
[61] J. Li, P. Stoica, and Z. Wang, "On robust Capon beamforming and diagonal loading," *IEEE Transactions on Signal Processing*, vol. 51, no. 7, pp. 1702–1715, 2003.
[62] S. A. Vorobyov, A. B. Gershman, and Z.-Q. Luo, "Robust adaptive beamforming using worst-case performance optimization: A solution to the signal mismatch problem," *IEEE Transactions on Signal Processing*, vol. 51, no. 2, pp. 313–324, 2003.
[63] O. Ronneberger, P. Fischer, and T. Brox, "U-net: Convolutional networks for biomedical image segmentation," in *Medical Image Computing and Computer-Assisted Intervention–MICCAI 2015: 18th International Conference, Munich, Germany, October 5-9, 2015, Proceedings, Part III 18*. Springer, 2015, pp. 234–241.
[64] C. Shorten and T. M. Khoshgoftaar, "A survey on image data augmentation for deep learning," *Journal of Big Data*, vol. 6, no. 1, pp. 1–48, 2019.
[65] M. Xue, L. Xu, and J. Li, "Iaa spectral estimation: fast implementation using the gohberg–semencul factorization," *IEEE Transactions on Signal Processing*, vol. 59, no. 7, pp. 3251–3261, 2011.
[66] G.-O. Glentis and A. Jakobsson, "Superfast approximative implementation of the iaa spectral estimate," *IEEE Transactions on Signal Processing*, vol. 60, no. 1, pp. 472–478, 2011.

Ruxin Zheng (Student Member, IEEE) received the B.S. degree in Electrical Engineering from the University of Pittsburgh, Pittsburgh, PA, USA, in 2018, the M.S. degree in Electrical Engineering from the University of Michigan, Ann Arbor, MI, USA, in 2020, and the Ph.D. degree in Electrical Engineering from the University of Alabama, Tuscaloosa, AL, USA, in 2025.

He is currently a Senior Technical Lead in Radar Systems at Aptiv, where he leads the development of next-generation automotive radar technologies. His research interests include automotive radar, radar signal processing, MIMO radar with sparse sensing, and model-based machine learning for signal reconstruction and perception.

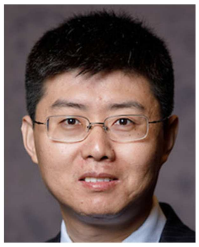

Shunqiao Sun (Senior Member, IEEE) received the Ph.D. degree in Electrical and Computer Engineering from Rutgers, The State University of New Jersey, New Brunswick, NJ, USA, in January 2016.

Dr. Sun is currently a tenure-track Assistant Professor at the Department of Electrical and Computer Engineering, The University of Alabama, Tuscaloosa, AL, USA. His research interests lie at the interface of statistical and sparse signal processing with mathematical optimizations, automotive radar, MIMO radar, machine learning, and smart sensing for autonomous vehicles. From 2016-2019, he was with the radar core team of Aptiv, Technical Center Malibu, California, where he has worked on advanced radar signal processing and machine learning algorithms for self-driving vehicles and lead the development of DOA estimation techniques for next-generation short-range radar sensor which has been used in over 120-million automotive radar units.

Dr. Sun received the U.S. National Science Foundation (NSF) CAREER Award (2024) and CRII Award (2022). He received the 2016 IEEE Aerospace and Electronics Systems Society (AESS) Robert T. Hill Best Dissertation Award for his thesis âMIMO radar with Sparse Sensingâ. He authored a paper that won the Best Student Paper Award at 2020 IEEE Sensor Array and Multichannel Signal Processing Workshop (SAM). He is an elected member of IEEE Sensor Array and Multichannel (SAM) Technical Committee (2024-2026), and an elected member of IEEE SPS Integrated Sensing and Communication Technical Working Group (2025-2027). He is Vice Chair of IEEE Signal Processing Society (SPS) Autonomous Systems Initiative (ASI) (2023-2025). He has co-organized the 1st, 2nd and 3rd Workshop on Signal Processing for Autonomous Systems (SPAS) at International Conference on Acoustics, Speech, and Signal Processing (ICASSP) 2023 in Rhodes, Greece, ICASSP 2024 in Seoul, Korea, and European Signal Processing Conference (EUSIPCO) 2025 in Palermo, Italy, respectively. He has co-organized 15 special/focused sessions on automotive radar signal processing, machine learning and sparse arrays at IEEE SPS and AESS flagship conferences. He is an Associate Editor of IEEE Signal Processing Letters and IEEE Open Journal of Signal Processing. He is a Senior Member of IEEE.

Hongshan Liu (Student Member, IEEE) received the B.S. degree in Physics from Zhejiang University, Hangzhou, China, in 2018, the M.S. degree in Electrical Engineering from the University of Michigan, Ann Arbor, MI, USA, in 2020, and the Ph.D. degree in Biomedical Engineering from Stevens Institute of Technology, Hoboken, NJ, USA, in 2024. Her research focuses on deep learning-based image processing and its applications in biomedical imaging.

Honglei Chen (Member, IEEE) received his B.S. degree from Beijing Institute of Technology and his M.S. and Ph.D. degrees from University of Massachusetts Dartmouth, all in Electrical Engineering.

Dr. Chen is a principal engineer at MathWorks where he leads the development of phased-array system simulation tools and algorithms for radar, 5G, sonar, and ultrasound applications.

Jian Li (Fellow, IEEE) received the M.Sc. and Ph.D. degrees in electrical engineering from The Ohio State University, Columbus, in 1987 and 1991, respectively.

She is currently a Professor in the Department of Electrical and Computer Engineering, University of Florida, Gainesville. Her current research interests include spectral estimation, statistical and array signal processing, and their applications to radar, sonar, and biomedical engineering. Dr. Li's publications include Robust Adaptive Beamforming (2005, Wiley), Spectral Analysis: the Missing Data Case (2005, Morgan & Claypool), MIMO Radar Signal Processing (2009, Wiley), and Waveform Design for Active Sensing Systems – A Computational Approach (2011, Cambridge University Press).

Dr. Li is a Fellow of IEEE and a Fellow of IET. She is a Fellow of the European Academy of Sciences (Brussels). She received the 1994 National Science Foundation Young Investigator Award and the 1996 Office of Naval Research Young Investigator Award. She was an Executive Committee Member of the 2002 International Conference on Acoustics, Speech, and Signal Processing, Orlando, Florida, May 2002. She was an Associate Editor of the IEEE Transactions on Signal Processing from 1999 to 2005, an Associate Editor of the IEEE Signal Processing Magazine from 2003 to 2005, and a member of the Editorial Board of Signal Processing, a publication of the European Association for Signal Processing (EURASIP), from 2005 to 2007. She was a member of the Editorial Board of the IEEE Signal Processing Magazine from 2010 to 2012. She is a co-author of the paper that has received the M. Barry Carlton Award for the best paper published in IEEE Transactions on Aerospace and Electronic Systems in 2005. She is also a co-author of a paper published in IEEE Transactions on Signal Processing that has received the Best Paper Award in 2013 from the IEEE Signal Processing Society.